Blade Lock Ring of 4th Stage Compressor Rotor: Failure Investigation

Aginaparru Sambasiva Rao and Ashok Kumar Singh

ABSTRACT

Present work describes the failure investigation of blade lock ring of 4th stage compressor rotor. The lock ring is fabricated from martensitic stainless steel. The microstructure of failed lock ring is tempered martensite. It shows non-metallic inclusions with three distinct shapes namely, elongated (MnS), globular (Al_2O_3) and complex shaped (oxy-sulphide). The corrosion pits and corrosion debris are observed in un-etched microstructure and fracture surface, respectively. The tree like branching cracks has observed at several places near surface. These cracks have initiated from the corrosion pits and then propagated inside the material. The interface of inclusions and matrix has also acted as crack initiator. The lock ring has initially suffered pitting corrosion in service and then cracks have propagated inside the material by stress corrosion cracking.

Keywords: Lock ring; Stainless steel; Inclusions; Pitting; Stress corrosion cracking.

1. INTRODUCTION

The main purpose of compressor rotor is to raise the pressure of incoming air to have an efficient combustion in the combustion chamber and to generate enough thrust to propel the aircraft [1]. Air entering the compressor section is compressed and delivered into the combustor section where it is mixed with fuel and then ignited to generate high-speed exhaust gas flow [2] .The compressor rotor blades from 4th to 9th stages are made up of Ni-base alloys. These are mounted to a fan hub and a blade lock assembly is used to axially retain the fan blades within corresponding fan hub slots. Blade lock assembly includes a lock ring that is axially slid onto the fan hub in an unlocked position and rotated to a locked position. This includes a fan hub that has blade slots each configured to receive a root of a fan blade. The locking ring includes circumferentially spaced second slots aligned with the first slots in the locked position and multiple discrete pins. Blade lock ring of 4th stage compressor rotor of aero engine had failed and found broken during overhauling. Total number of hours utilized the existing lock ring since new is 931:29 hours. However, expected life of the lock ring as per specification is 1500 hrs. Present work describes the metallurgical failure analysis of blade lock ring of 4th stage compressor rotor which was pre-maturely failed.

2. EXPERIMENTAL

Initially, the failed blade lock ring segments were examined visually and photographs of failed ends as well as typical flat surfaces of both the parts were captured using high resolution digital camera in as-received condition. In order to examine the surface cracks (if any) on the flat surface of failed ring, non-destructive test was carried out on both sides of plane surfaces using dye penetrate test. Drillings were taken from the region slightly away from the failed region for wet chemical analysis. In addition, small pieces of about 3×4 mm² size were also cut for carbon and sulphur analysis. Bulk chemical composition was analysed using inductively coupled plasma-optical emission spectroscopy (ICP-OES). The interstitial elements such as C and S were measured using inert gas fusion technique.

Samples were cut from the failed region and mounted its plane surface in Bakalite mounts in order to examine the microstructure under optical and scanning electron microscopes (OM and SEM).These samples were mounted and prepared using standard metallographic procedure. Surface irregularities near failed region and morphology of non-metallic inclusions (if any) were examined in as-polished samples using optical microscope in an un-etched condition. The polished samples were further etched with aquaregia (50% HCl and 50% HNO_3 by volume) and microstructural characterization was done using optical microscope. Samples were cut from the fracture ends of both the counter parts of failed lock ring and cleaned ultrasonically in acetone to remove dirt and other residues

A. S. Rao and A. K. Singh✉
Defence Metallurgical Research Laboratory
Kanchanbagh, Hyderabad, 500058, India
E-mail: singh_ashok3@rediffmail.com

over the fracture surface. Fracture surfaces were studied using FEI make environmental SEM (Model: Quanta 400) in secondary electron (SE) mode. Energy dispersive spectroscopy (EDS) was employed to evaluate the contaminated products over the fracture surfaces. Longitudinal sections of as-polished samples obtained from close to fracture as well as away from the failed region were also examined using CAMECA make, SX-100 model electron probe micro analyser (EPMA) in un-etched condition. In order to confirm the type and morphology of inclusions in the failed lock ring, X-ray elemental distribution mappings were carried out using EPMA technique. X-ray mappings of Mn, S, Al, Si and O elements were carried out at 20 kV and 20 nA current. X-ray elemental mappings were gathered for each element separately and correlated with respective back scattered electron (BSE) image for interpretation. Hardness measurements were carried out using Vickers hardness tester with 30 kg load. The hardness values were reported after taking an average of 10 measurements.

3. RESULTS

3.1. Visual Examination

Photograph of broken lock ring in as-received condition is shown in Fig. 1. The ring is in the form of flat surface all around the circumference. The width and the thickness of the lock ring are 5.5 and 2.5 mm, respectively. It clearly shows that the lock ring has broken into two pieces. These rings are smooth and shiny surface finish on both plane surfaces. It also exhibits several micro-cracks along one side of plane surface of the both parts of lock rings and are extended from one end to other end (Fig. 2a). These cracks are confirmed by dye penetrate (DP) test and also with stereo microscopic examinations (Figs. 2a and 3). Close inspection of the fracture surface in stereo microscope of failed lock ring displays two distinct features with dark and bright contrast (Fig. 2b). The major part (~75%) of the fracture surface exhibits dull and dark contrast while the remaining part (~25%) is bright and shiny.
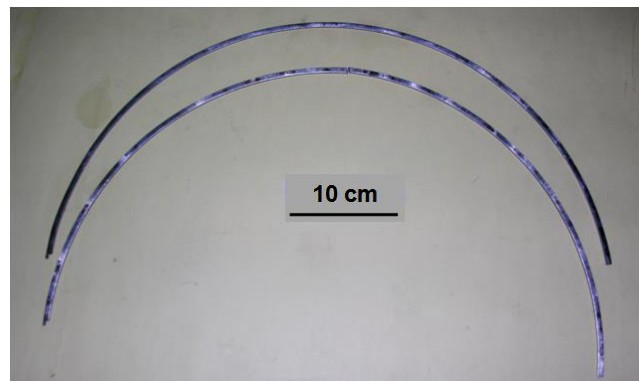
Figure.1: Broken parts of lock ring in as-received condition.
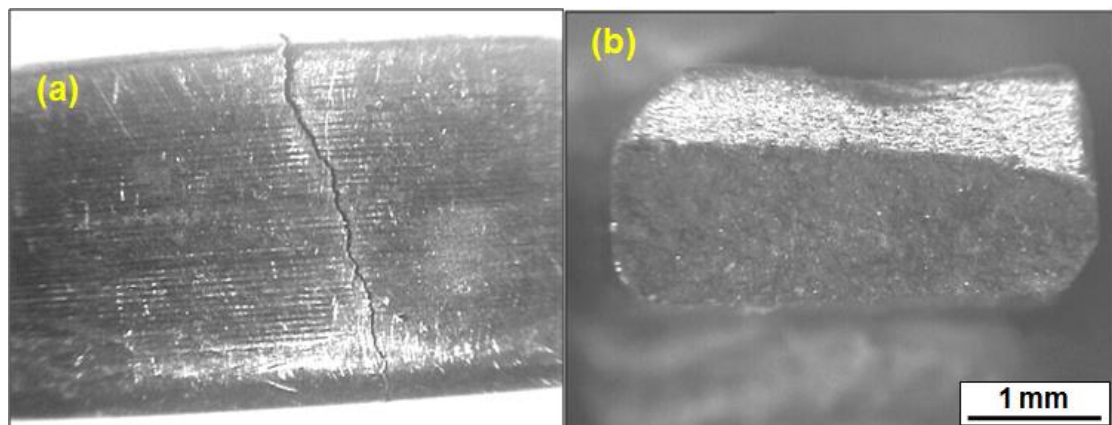
Figure. 2: Stereo micrographs of failed lock ring: (a) irregular crack across the width on one plane surface and (b) dark and bright fracture surface obtained from broken lock ring.
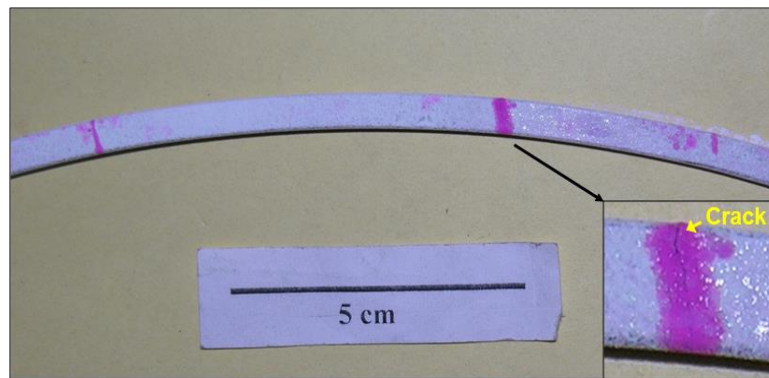
Figure.3: Photograph of post dye penetrant test showing several cracks across the width on one plane surface of failed lock ring (magnified image of crack region is shown as inset).
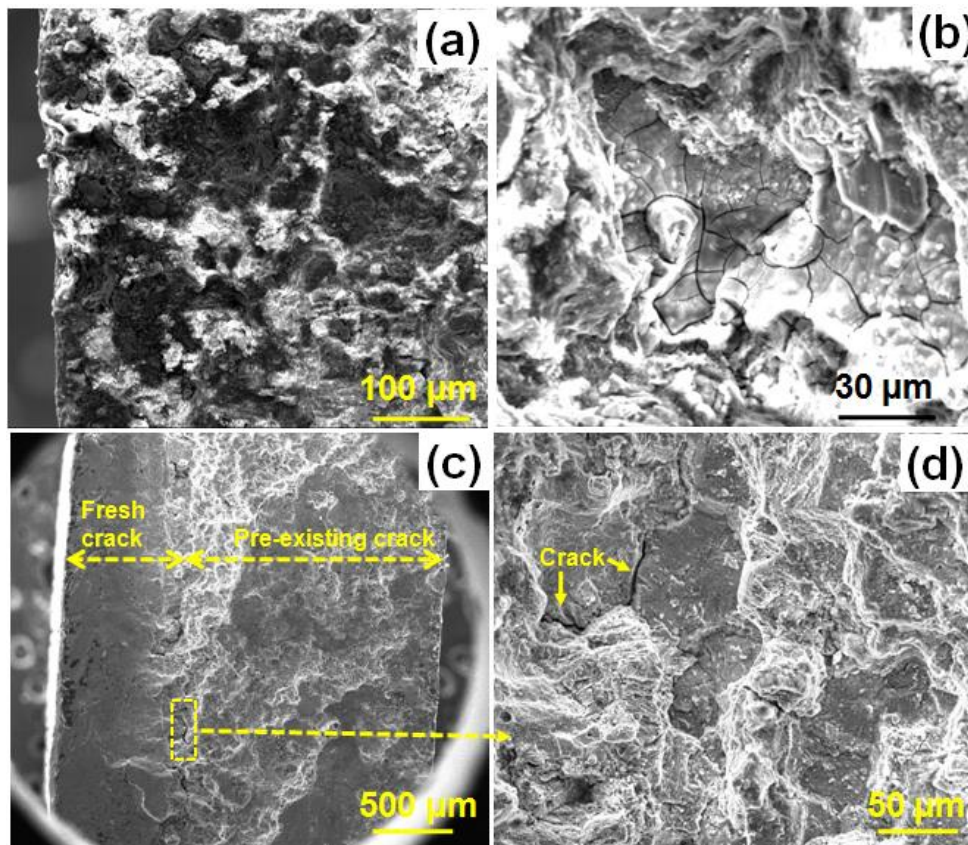
Figure. 4: SEM fractographs: (a) fracture features from dark region, (b) magnified image of (a) reveals several mud cracks, (c) fracture surface of entire fracture surface with distinct regions and (d) magnified image of (c) from mating surface between dark and bright regions.

3.2. SEM Fractography

SE images of fracture surface corresponds to entire fracture area has been examined and the fractographs taken at different magnifications are shown in Fig. 4. The fracture characteristics of dark region are quite different from that of the bright region. Specifically, thick layer of contaminated foreign material has masked over the dark region of fracture surface (Fig. 4a). Magnified micrograph of the dark region demonstrates extensive mud cracks which are typical of corrosion derbies (Fig. 4b). On the contrary, bright region of fracture surface reveals cleavage facets (Fig. 4 c and d). It also illustrates grain boundary cracks close to the mating surface between dark and bright fracture regions (Fig. 4 c and d).

3.3. Energy Dispersive Spectroscopy (EDS)

EDS analysis was carried out on the dark region of the fracture surface. The EDS spectrum reveals the presence of C, O, Ca, Cl, Na, Mg, Al, Si and K along with elements pertaining to parent material (Fig. 5). This also confirms that the dark fracture region is enveloped with corrosion products.

3.4. Optical Microstructure

Longitudinal samples prepared from plane surface of failed lock ring exhibits typical tempered martensite structure in-etched condition (Fig. 6). The microstructure of the samples close to fracture surface in un-etched condition is shown in Fig. 7. Surface close to outermost edge exhibits surface pitting at several locations. It indicates that the material was degraded during service and also part of the same has dislodged from the parent material due to localized pitting. The formation of pitting is quite severe at the surface than that of the interior of the lock ring.
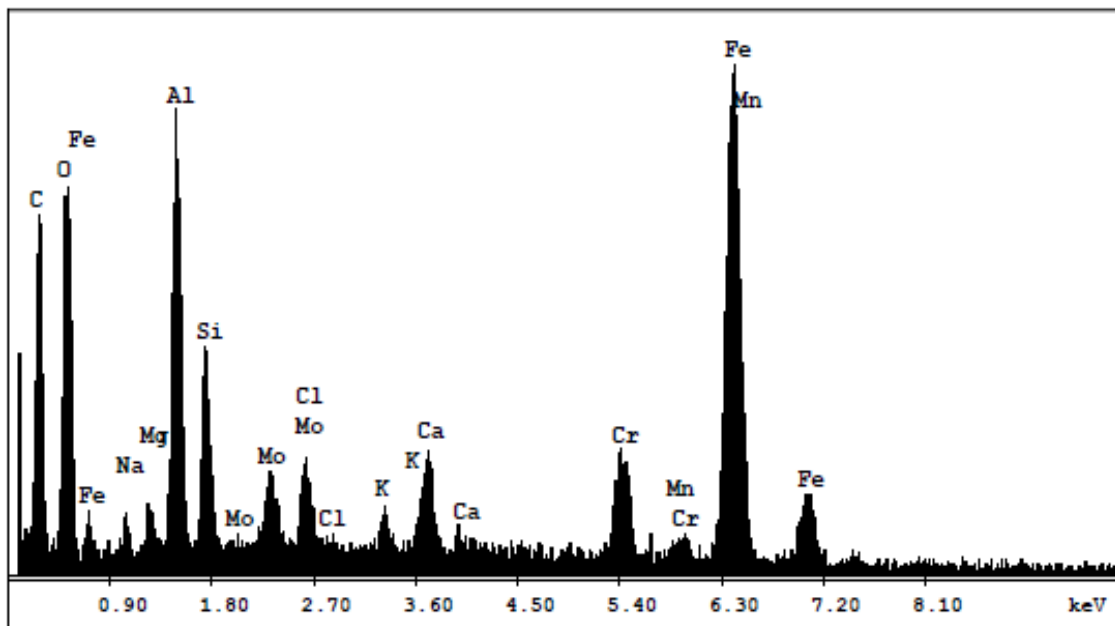
Figure. 5: EDS spectrum of the dark region of fracture surface showing corrosion products along with major elements of parent material.
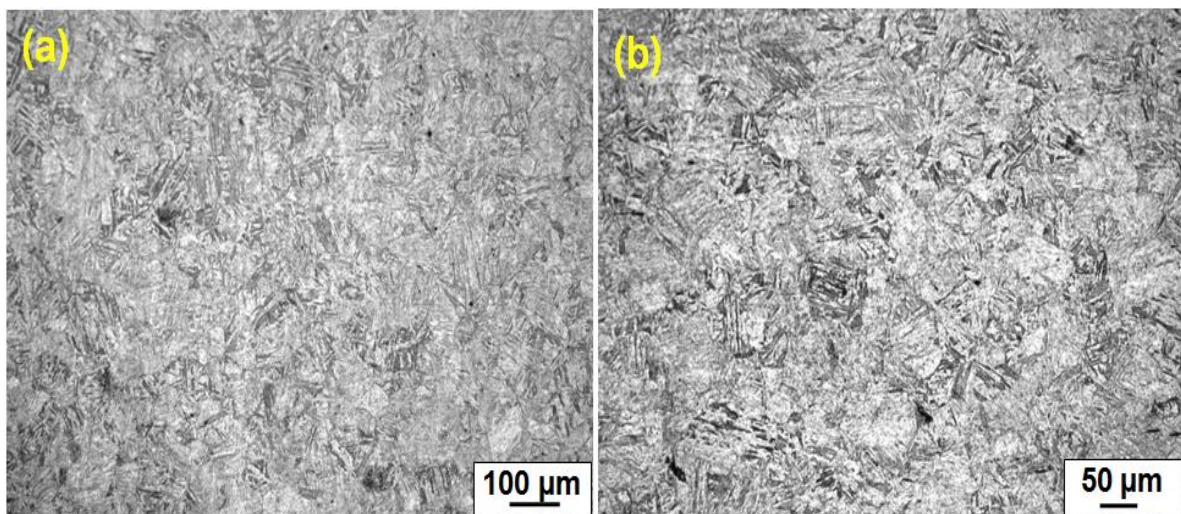
Figure. 6: Microstructures showing tempered martensite: (a) low and (b) high magnifications.
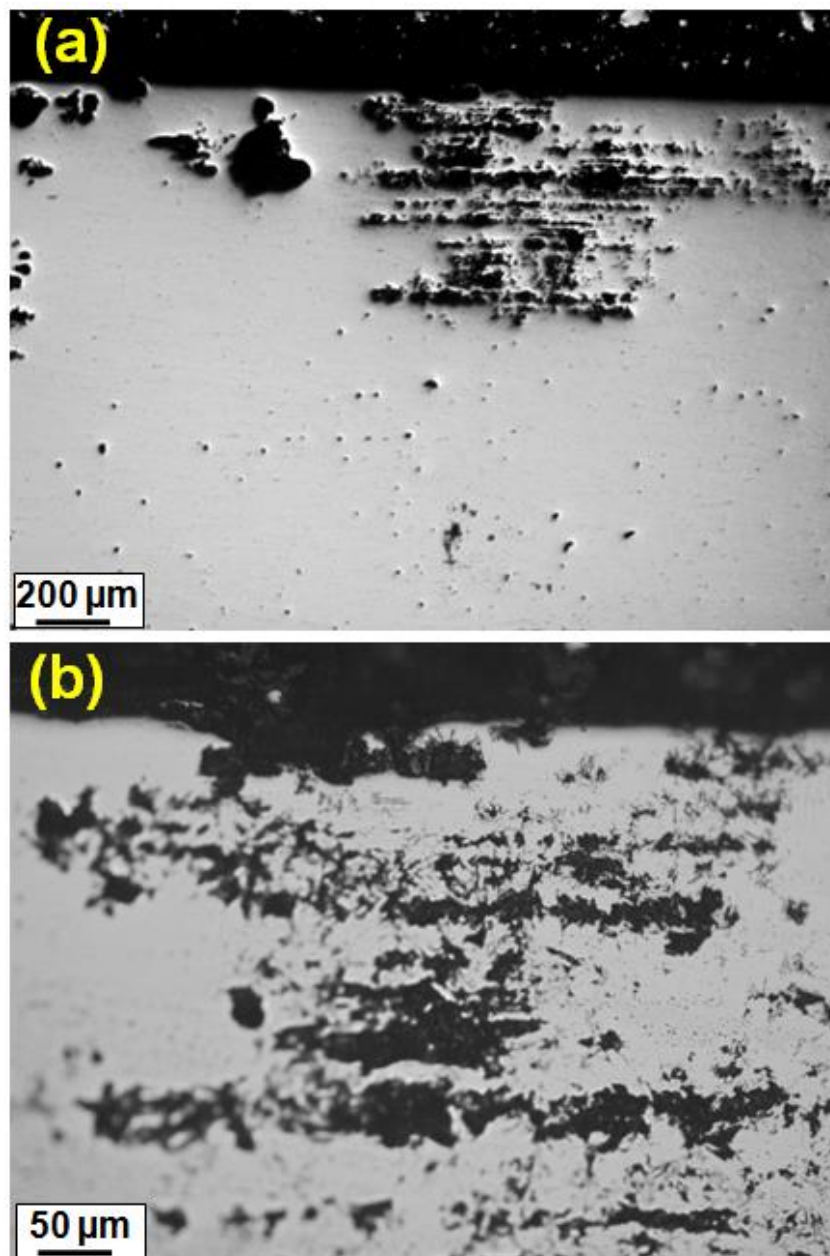
Figure. 7: Optical microstructures of failed lock ring close to surface exhibits pitting cavities in un-etched condition: (a) low and (b) high magnifications.

3.5. Electron Probe Micro Analyser (EPMA)
3.5.1. Back Scattered Electron Images

Back scattered electron images obtained from the failed lock ring close to fracture region demonstrates extensive pitting at several locations near the top surface (Fig. 8). These features are similar to those observed in optical microscope. This also confirms that the material has undergone pitting corrosion which has initiated at the surface. In addition, the cracks which are originated from the plane surface of its width side have further propagated into the base material along with several branches (Fig. 8). Low magnification BSE image obtained for entire width of the failed lock ring part exhibits abundant number of cracks with multi-branching. These cracks are extended towards inside the material (Fig. 9a). Magnified microstructures taken from three different regions of Fig. 9a clearly indicate that the cracks have propagated arbitrarily into different directions and formed tree like branching (Fig. 9 b-d). As a result, part of the base material has also dislodged from the affected area.
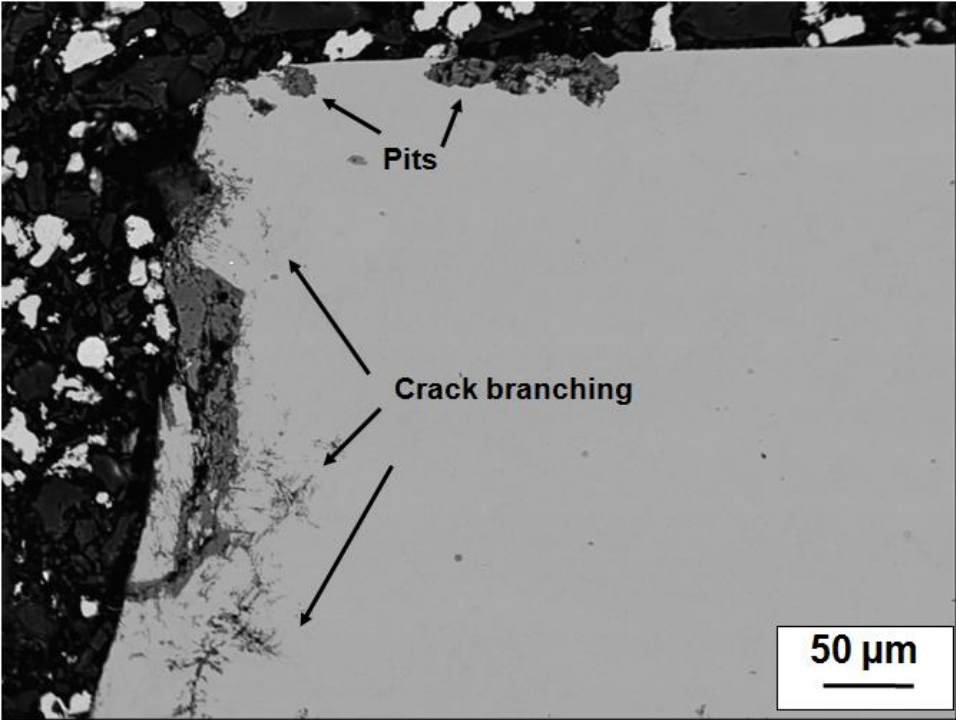
Figure. 8: EPMA-BSE image at crack tip of the failed lock ring.
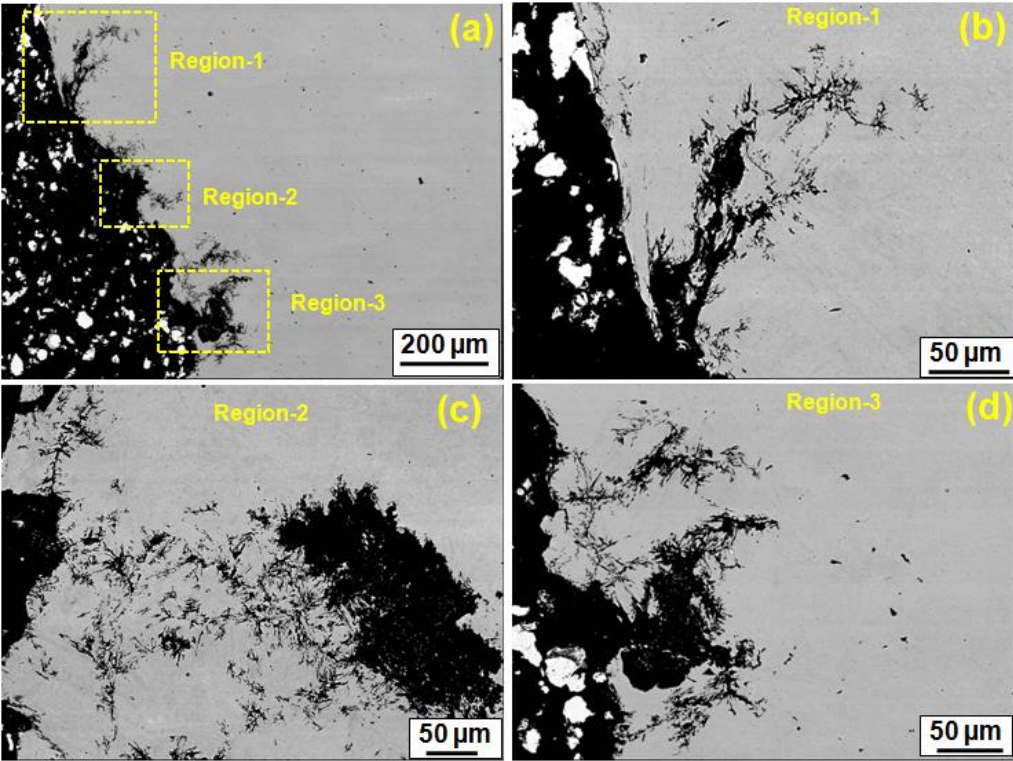
Figure. 9: EPMA-BSE images: (a) low magnified image for entire width of failed ring, (b), (c) and (d) magnified images obtained from different region of (a).

3.5.2. X-ray Elemental Distribution Mappings

BSE image of failed lock ring exhibits the presence of both the elongated as well as globular inclusions. In order to identify the type and its morphology, X-ray elemental distribution mappings are obtained at three different regions and shown in Figs. 10-12. The base material reveals elongated manganese sulphide inclusions (Fig. 10). These MnS inclusions are elongated along the rolling direction and are located as bunch of inclusions within the area of about $200 \times 200\ \mu m^2$ area.

Another set of X-ray elemental distribution mappings has been taken from the region wherein both the elongated and globular inclusions are present. These mappings reveal the enrichment of O, Al and Mn, S elements, respectively (Fig. 11). This reflects that the MnS and Al_2O_3 types of inclusions are predominantly present in the material. X-ray mappings are also gathered from the region wherein both the types of inclusions are imbedded as single identity. It clearly illustrates that globular oxide inclusion is encapsulated with elongated MnS (Fig. 12). The MnS inclusion is elongated and located at the periphery of the Al_2O_3. EPMA analysis shows that the parent material used for lock ring contains predominantly MnS as well as Al_2O_3 types of inclusions.
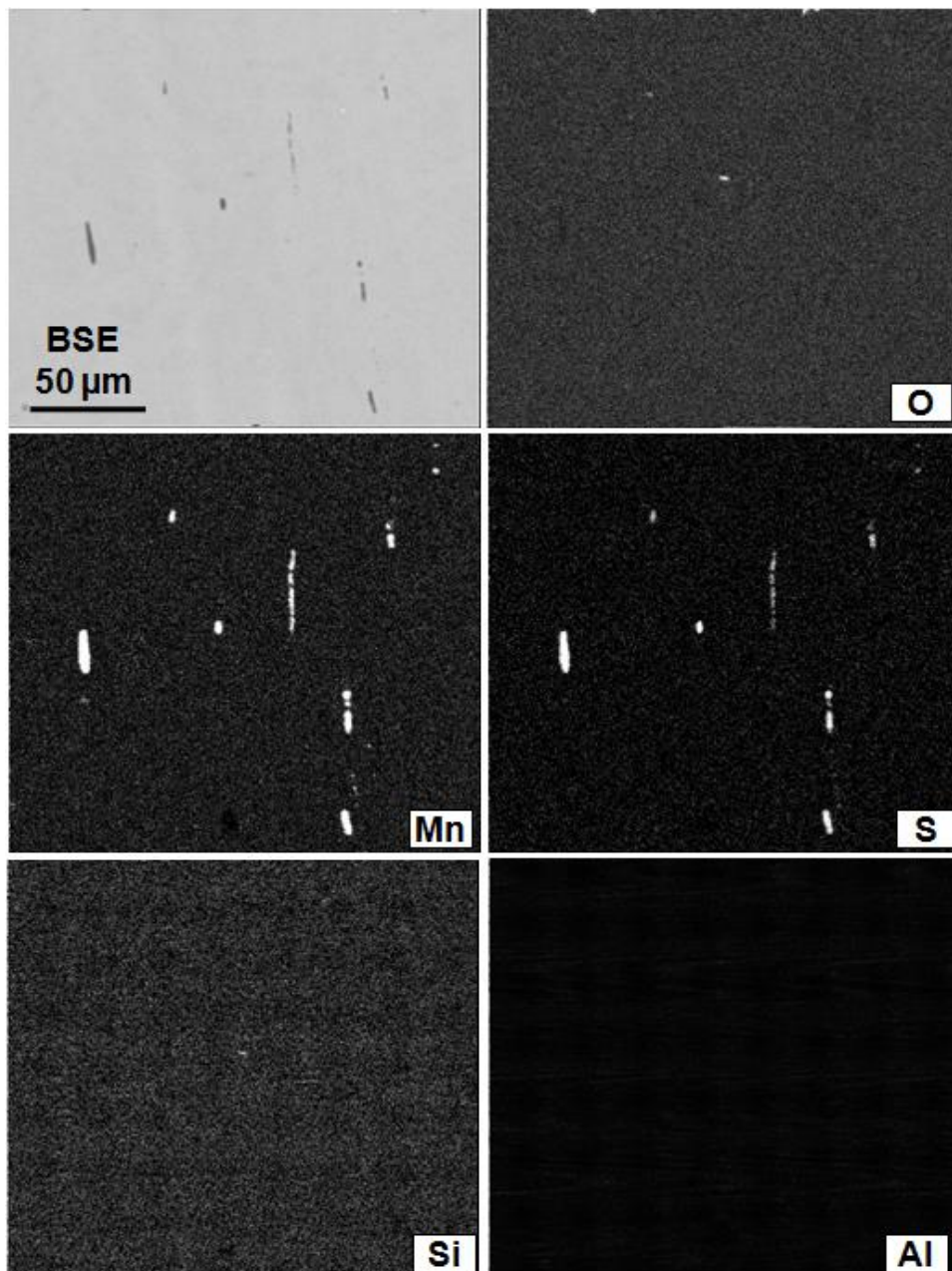
Figure. 10: EPMA X-ray elemental distribution mappings of the elements Mn, S, O and Al.
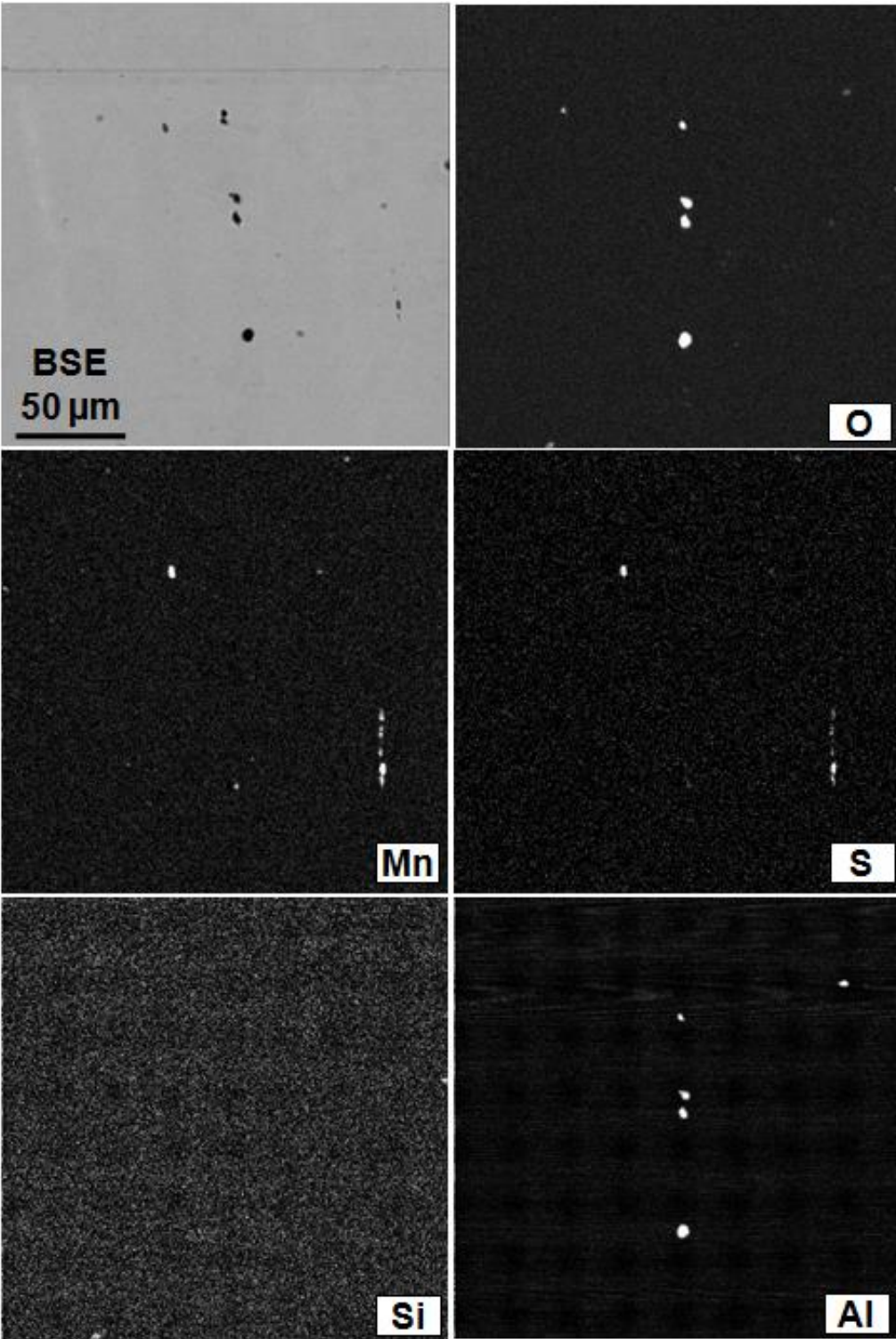
Figure. 11: EPMA X-ray elemental distribution mappings of the elements Mn, S, O, Si and Al.
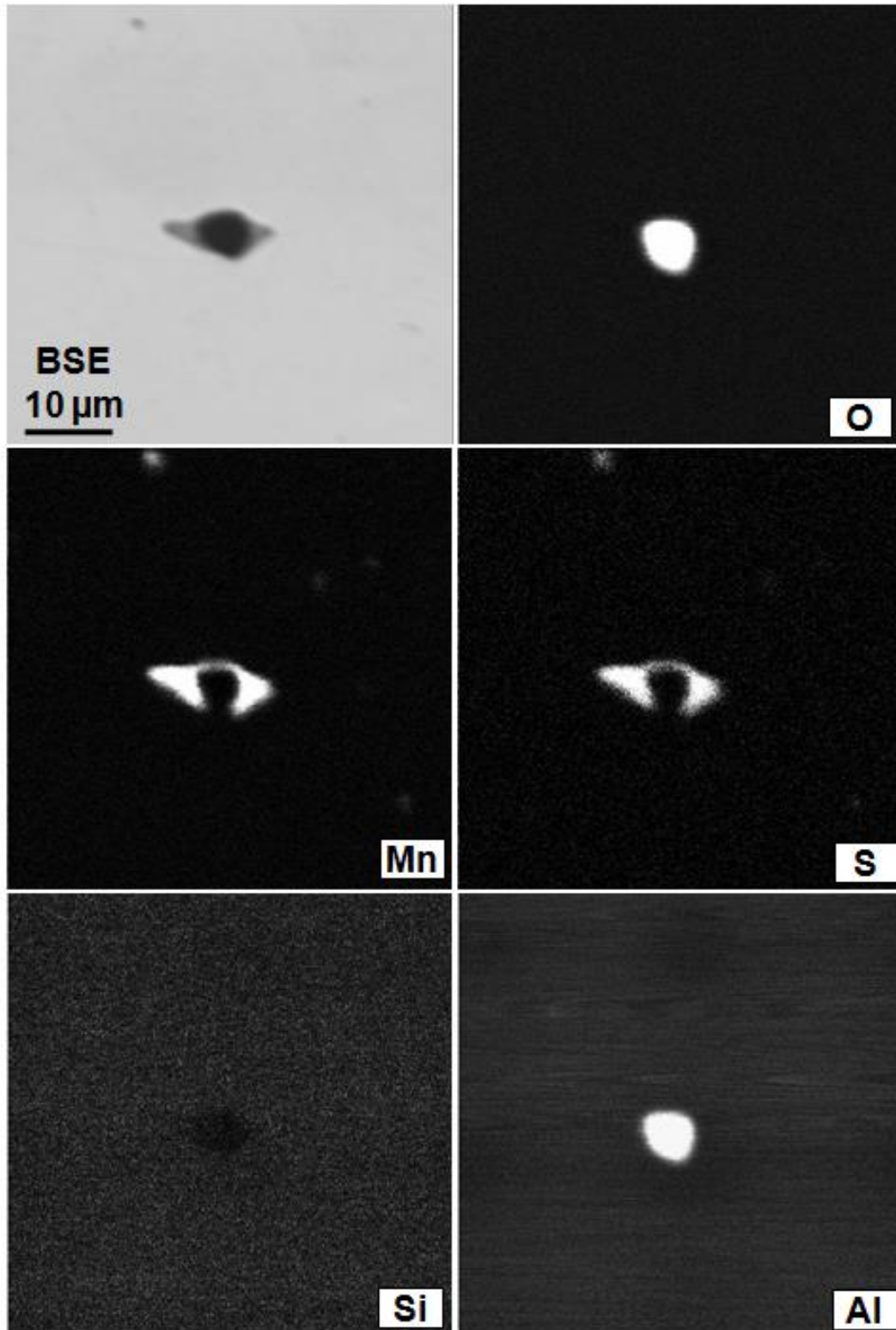
Figure. 12: EPMA X-ray elemental distribution mappings of the elements Mn, S, O, Si and Al.

3.6. Chemical Composition and Hardness

The chemical composition of the lock ring obtained by ICP-OES technique is given in Table 1. The interstitial elements C and S are also included in Table 1. The chemical composition of the lock ring is similar to that of the martensitic stainless steel (AISI 422) [3]. The hardness value of the failed lock ring is ~390 ± 5 VHN_{30}.

Table 1: Chemical composition of the lock ring

Element	C	S	Ni	Cr	Mn	Mo	V	W	Fe
wt. %	0.105	0.009	1.66	10.78	0.4	0.39	0.21	1.75	Balance

4. DISCUSSIONS

Chemical composition of the lock ring sample suggests that it is made up of martensitic Stainless Steel. The analysed composition is nearly equivalent to AISI 422 grade. Alloy AISI 422 is a hardenable stainless steel designed for use up to 649 °C. The properties can be optimized through heat treatment (hardening and tempering). As this material is resistance to scaling and oxidation and also having high strength, it is a potential candidate for fabricating aircraft components [3-4]. Both the microstructure and hardness indicate that the lock ring material is in hardened and tempered condition.

The failed lock ring contains a large amount of non-metallic inclusions with three distinct shapes. These are elongated (MnS), globular (Al_2O_3) and a complex shape wherein Al_2O_3 is embedded with MnS called as oxy-sulphide. It is to be noted that these inclusions are not permitted for aerospace applications, as they reduce the mechanical properties and corrosion resistance of the material.

The surface of the lock ring has suffered severe pitting corrosion as evidenced by metallography and EPMA studies. Several branching cracks are found propagating from the corrosion pits into the material which point towards the occurrence of stress-corrosion cracking (SCC). Dark contrast with mud cracks on 75% of the fracture surface reflects that these cracks were open to corrosion environment during service. The EDS results also confirm the same. SEM micrograph of the fracture surface exhibits extensive mud-cracks which has masked the most of the fracture features (Fig.4 b). These mud-cracks are the characteristics of drying out of hydrated, probably gel-like deposits. Hence, mud-cracks are typically termed as corrosion debris. In addition mud-crack pattern can usually be seen on fracture surfaces caused by SCC and SEM fractography study is required to see the mud-crack pattern in most cases [5]. The fracture region close to mating surface of pre-existing crack and newly formed crack reveals cleavage facets (Fig. 4 c and d). This indicates that the material has failed in brittle manner. Interestingly, cleavage mode of brittle fracture feature is one of the characteristic of SCC [6].

As reported by Truhan et al., a very close relationship exists between stress corrosion cracking and pitting [7]. It is known that stainless steel forms chromium oxide passive film to protect from environmental corrosion. As a result, the components made up of stainless steel material are less susceptible to corrosion during service [8]. However, if the passive film damages or breaks due to other service / environmental conditions, then it lead to the creation of local anodes surrounded by relatively large cathodic areas of matrix material and pitting results. In addition, the areas which are formed as anodic to act as initiator for pitting have been identified as metal carbides, sulphide inclusion, grain boundaries and deformed material. More likely processes for premature passive film breakdown are: (i) mechanical breakdown of the passive film, (ii) chloride adsorption to change the conductivity properties of the film and (iii) preferential dissolution of certain precipitates / sulphides [7]. Once localized breakdown of the passive film occurs, these small discontinuities acts as relatively anodic and then these areas become prone to pitting. Pitting corrosion is therefore, an electrochemical oxidation-reduction process, which occurs within localized deeps on the surface of metals coated with a passive film [9]. The corresponding anodic reaction inside the pit is given below.

$$Fe = Fe^{2+} + 2e^{-} \text{ (dissolution of iron)} \qquad (1)$$

These pits cause failure through perforation (a small hole or row of small holes) and engender stress corrosion cracks. Subsequently, the life cycles of stainless alloy components decrease [9]. Stress corrosion cracking (SCC) may initiate at the base of corrosion pits and then propagate inside the material [5 and 10]. The SCC cracking may be defined as the delayed failure of alloys by cracking when exposed to certain environments in the presence of a static / residual tensile stress [6]. SCC is the cracking induced from the combined influence of tensile stress and a corrosive medium.

As the lock ring is utilized to lock the blades in 4th stage compressor rotor, it has been subjected to continuous tensile stress during operation. In addition, the environmental condition during operation/service might have provoked to initiate stress corrosion. Thus the failed lock ring exhibits several tree like branched cracks which have been initiated from surface and then propagated inside the material. This has subsequently broken the lock ring into two pieces. Similar type of tree branched cracks have been observed for the stainless steel material failed due to stress corrosion cracking [11].

The SCC frequently initiates at pre-existing feature. It includes groves, laps, burs and / or stress concentrated sharp corners etc. [12]. In addition, the SCC can also initiate at pits that are formed during exposure to service environment. Pits can form at inclusions that intersect the free surface. Secondary phases, like MnS inclusions act as crack initiation sites by promoting localized corrosion of the material [13]. It is also reported that sulphide inclusions act as anodic relative to the surrounding sulphur free matrix [13]. Thus, MnS inclusion decreases the pitting resistance of the material. Frankel has also stated that the pits in stainless steels are often associated with

MnS inclusions [14]. Once the crack reaches a critical crack length, it continues to propagate the metal and the reminder of the fracture surface fails. It is also reported by Liu et al. that the pitting corrosion occurs preferentially around the Al_2O_3 inclusions. As Al_2O_3 inclusions are stable and hard, during the process of corrosion, these inclusions do not dissolve like MnS [15]. Therefore, pitting corrosion is induced at the interface of the inclusions and the steel matrix and then results in micro cracks. As the corrosion progressed, the size of the micro-crack becomes larger and accordingly cracks progress inside the material. Both the elongated MnS and globular Al_2O_3 inclusions aggravate the stress concentration sites to initiate the SCC. The oxy-sulphide inclusion observed in EPMA mapping has been reported in stainless steel by Grajcar et al. [16]. These inclusions also act as preferential sites for pit formation and corrosion pitting and nucleate at the interface between inclusion and matrix.

Present results have therefore pointed towards that the lock ring has initially suffered pitting corrosion in service and then cracks have propagated inside the material by stress corrosion cracking. This has introduced premature failure of lock ring during service.

5. CONCLUSIONS

This research showed the followings.
1. Lock ring has suffered with pre-existing cracks up to 3/4th of the thickness during service.
2. Complex type (oxy-sulphide) inclusions have changed the local crack-tip chemistry and acted as preferential sites for nucleation of pits at the interface between inclusions and matrix.
3. Crack with tree like multi-branching observed in failed lock ring is a key characteristic of stress corrosion cracking.
4. The lock ring has finally failed due to stress corrosion cracking that has initiated due to pitting corrosion.

ACKNOWLEDGEMENTS

REFERENCES

1. Mallikarjuna, V., Kishore, G. K. and Reddy, B. R. B. (2013). Fatigue analysis and design of different compressor rotor blade of an Orpheus engine, International journal of advanced research in engineering and applied sciences, 2(9), 40-55.
2. Andeson, C. R. and Tomeo, P. V. (2014). Gas turbine engine fan blade lock assembly, U S Patent US2014/0133991 A1.
3. Hamilton, M. L., Huang, F. H.and Hu, W. (1992). Mechanical properties of martensitic allot AISI 422, Presented at the 16th ASTM international conference on radiation effect on materials, Denver, Colorado.
4. Stainless steel 422 / S42200 / 1.4935 / 616, http://4.imimg.com/data4/KG/VI/MY-626992/stainless-steel-422-round-bar.pdf.
5. Brown, B. F. (1977). Stress corrosion cracking control measures, National bureau of standards monograph 156.
6. Chatterjee, U. K. (1995).Stress corrosion cracking and component failure: Causes and prevention, Sadhana, 20(1), 165-184.
7. Truhan, J.J., Jr. and Hehemann, R.F. (1977). Surface aspects of pitting and stress corrosion cracking, Case Western Reserve University, Cleveland, Ohio, prepared by National aeronautics and space administration NASA Lewis research centre, Grant NGR 36-027-051.
8. Leffler, B. (1998). Stainless-stainless steels and their properties. Chapter 3. 2nd edition.
9. Bensalah, N. (2012). Pitting corrosion. Chapter 7, Corrosive effects of chlorides on metals, Fong-Yuan Ma. Chaina.
10. Roberge, P.R. (2012). Handbook of corrosion engineering, McGraw-Hill, New York San Francisco, Chapter 5, Corrosion failure, 332.
11. Aly, O.F. and Neto, M.M. (2013). Stress corrosion cracking, Chapter 4, Developments in corrosion protection, ed. M Aliofkhazraei, Intech Open publishers, 65-79. http://dx.doi.org/10.5772/57349
12. Jones, R. H. (2017). Stress-corrosion cracking, Materials performance and evaluation, second edition, Chapter 1, Mechanism of stress-corrosion cracking, ASM International.
13. Gulbrandsen, S. (2012). Stress corrosion cracking of 316L austenitic Stainless steel in high temperature ethanol/water environments, Thesis on Degree Master of Science in the School of Materials Science and Engineering, Georgia Institute of Technology.
14. Frankel, G. S. (1998). Pitting Corrosion of Metals A Review of the Critical Factors, Journal of the Electrochemical Society, 145(6), 2186-2198. DOI: 10.1149/1.1838615
15. Liu, Q., Yang, S., Zhao, M., Zhu, L. and Li, J. (2017). Pitting Corrosion of Steel Induced by Al_2O_3 Inclusions, Metals, 7(247), 1-12. doi:10.3390/met7090347.
16. Grajcar, A. and Plachciñska, A. (2016).Effect of sulphide inclusions on the Pitting-corrosion behaviour of high-Mn steels in Chloride and alkaline solutions, Materials and technology 50 (5), 713–718. DOI: 10.17222/mit.2015.169